

# Models in Computational Turbulent Flows

Zeyu Jia\*      Zhihan Li\*

1600010603    1600010653

June 19, 2018

## Abstract

Fluid, highly versatile, have both global structures and time-varying details. This results in difficulties for computation and modeling. In spite of such challenges, *computational fluid dynamics* (CFD) has attracted attention since 20<sup>th</sup> century, and lots of methodologies have been developed due to the huge number of applications of fluids in engineering. Among different kinds of computational fluid dynamics tasks, *turbulent flows* are of high importance because of its universality and complexity. In order to achieve computational possibility, lots of simplified turbulent models have been proposed. In this report, we investigate and summarize three main types of turbulent models: *direct numerical simulation* (DNS) models, *large eddy simulation* (LES) models and *Reynolds-averaged simulation* (RAS) models. We provide detailed analysis and numerical experiments for comparison. We show that these three kinds of models enjoy different precision and efficiency, and therefore fit in different cases. The project is held on <https://github.com/pppppass/TurbulentFlow>, with the report <https://github.com/pppppass/TurbulentFlow/Report/Report.pdf> in digital version.

## 1 Introduction

*Fluids* are an important subset of phases of matter. The key distinction between fluids and solids are there response to shear forces: shear stress comes in to place in resistance for solids, according to shear modulus; while an absence of such stress results in fluids [2]. In some sense, fluids can be deformed “freely”. Liquids and gases exemplify fluids in every day life.

Equations of fluid motion have been well established, including the continuity equation and the famous Navier–Stokes equations, which reflect the conservation of mass and momentum

---

\*Equal contribution.

respectively [5] [10]. These equations bring opportunities for computational fluid dynamics and fluid simulation. However, because the momentum itself affects flow velocity, the system goes non-linear, and no theorem about existence and uniqueness of solution for general cases has been proven yet [11].

Because of the freedom of deformation, fluids may have relatively stable global structures in a large scale, while local structures can be space and time-varying. This means fluids enjoy a nature of multi-scale. This leads to difficulties for numerical simulation of fluids, because a grid capturing both coarse and fine structures is bound to have some density.

*Turbulent flow*, or say turbulence, is a kind of flow phenomena, on the contrary to laminar flow. For laminar flows, the flow can be divided into parallel layers, and the flow velocity remains relatively stable. However, in turbulent flow cases, the flow is highly unsteady and the flow velocity changes rapidly. It is said that turbulent flow boost the process of mixing by breaking volumes of different properties into small pieces and enlarging the interaction surface. In this sense, *turbulent diffusion* can be considered [2]. A prominent property for turbulent flows is chaos: tiny changes of the initial condition may result in completely different patterns. Another property is the change in vorticity, which always lead to different sizes of vortexes and even vortex streets [2].

Because of the chaotic behavior, it is rather complicated to derive properties of general turbulent flows directly from governing equations. Therefore, simplified and statistical models have also been investigated, especially from the communities of physics and probability theory. One of the most famous models is the *energy cascade model* for local isotropic turbulent flows by Richardson [8], which emphasizes the similarity between turbulent flows of different scales. In this model, turbulent flows of large scales contain much energy, and they gets broken up and reach relatively equilibrium, and finally enter the dissipation range of scales. Kolmogorov further established concrete hypothesis for these models, and proposed the famous  $-5/3$  spectra, which claims the existence of curve segment of slope  $-5/3$  in normalized energy spectra [4]. This phenomena is checked by many experiments, and universality has been verified [7].

On the computational side, there are also simplifications on models designed specially for numerical simulation. There are mainly three categories for corresponding models and algorithms:

- (1) Direct numerical simulation (DNS): directly simulate the turbulent flow according to Navier–Stokes equations, with the fluids model completely unchanged.
- (2) Large eddy simulation (LES): solve only the large-scale part of motion while approximation the scale-scale one.
- (3) Reynolds-averaged simulation (RAS): make advantage of statistical steadiness of the chaotic system and solve the time-averaged equations.

Each model have pros and cons of itself, and this will be analyzed in later sections.

The plan of this report is as follows. We will introduce basic concepts and equations of

fluid dynamics in Section 1 and 2. Different models, say DNS, LES and RAS will be detailedly discussed in Section 3, 4 and 5 respectively. We will conduct a full comparison of these three models in 6, with analysis and experiments provided. Conclusion will be given in Section 7, with acknowledgement Section 8.

The main contents of models are summarized from [6] [11]. Some analysis are made originally.

## 2 Equations of fluid motion

### 2.1 Incompressible Naiver–Stokes equations

We first establish equations of fluid motion [6] [2], as a preparation of further discussion.

Denote density of the fluid as a scalar function  $\rho$  with respect to the time and position  $(t, \mathbf{x}) \in \mathbb{R}^{3+1}$ . We also denote flow velocity as a vector function  $\mathbf{U}$  similarly.

We proceed consider the Lagrangian coordinate first. For a given point  $\mathbf{x}$ , we can solve for its trajectory  $\mathbf{X}(t, \mathbf{x})$  according to the velocity field from the equation

$$\frac{\partial}{\partial t} \mathbf{X}(t, \mathbf{x}) = \mathbf{U}(t, \mathbf{X}(t, \mathbf{x})). \quad (1)$$

Here  $\mathbf{X}$  is considered to be *Lagrangian coordinate*, in accordance to *Eulerian coordinate*  $\mathbf{x}$ . Lagrange coordinate provides use a map

$$\Phi^t(\mathbf{x}) = \mathbf{X}(t, \mathbf{x}), \quad (2)$$

which characterized the “deformation” from time 0 to  $t$ . When the fluid is completely steady, say  $\mathbf{U}$  is independent of time, this notation coincides with the one in dynamic systems.

For *control volume* (CV), which is a simply connected region with piece-wise smooth boundary,  $\Omega^0$ , we may consider the corresponding *control mass* (CM), which is the region evolving as  $\mathbf{U}$ . Mathematically, the control mass

$$\Omega^t = \Phi^t(\Omega^0). \quad (3)$$

For an intensive property  $\phi$ , a scalar or a vector, we have

$$\frac{d}{dt} \int_{\Omega^t} \rho \phi d\Omega = \frac{d}{dt} \int_{\Omega^0} \rho \phi d\Omega + \int_{\partial \Omega^0} \rho \phi \mathbf{U} \cdot d\mathbf{S}. \quad (4)$$

If  $\phi$  is itself conserved, we have integral conservation law

$$\frac{d}{dt} \int_{\Omega^0} \rho \phi d\Omega + \int_{\partial \Omega^0} \rho \phi \mathbf{U} \cdot d\mathbf{S} = \Gamma. \quad (5)$$

For the differential one, we may introduce *material derivative*

$$\frac{D}{Dt} = \frac{\partial}{\partial t} + \mathbf{U} \cdot \nabla, \quad (6)$$

and the conservation law turns out to be

$$\frac{\partial \rho \phi}{\partial t} + \nabla \cdot (\rho \phi \mathbf{U}) = \frac{D \rho \phi}{Dt} + \rho \phi \nabla \cdot \mathbf{U} = \gamma, \quad (7)$$

where  $\gamma$  mirrors the change of  $\phi$  in infinitesimal control mass.

We begin to derive basic equations of fluid motion now. The basic one is the *continuity equation*, which pays attention on mass conservation. If we set  $\phi = 1$ , we obtain

$$\frac{d}{dt} \int_{\Omega^0} \rho d\Omega + \int_{\partial\Omega^0} \rho \mathbf{U} \cdot d\mathbf{S} = 0, \quad (8)$$

$$\frac{\partial \rho}{\partial t} + \nabla \cdot (\rho \mathbf{U}) = 0. \quad (9)$$

In the following discourse, we focus on *incompressible fluids* or *solenoidal fluids*, which means the divergence of flow velocity is always zero. There are also some other characterization of the incompressibility, as the following theorem tells. Under daily pressure, liquids like water can be considered to be incompressible, and accounts for popularity of incompressible models.

**Theorem 1** For a fluid satisfying continuity equation, the following are equivalent:

- (1) The flow velocity field is divergence-free:  $\nabla \cdot \mathbf{U} = 0$ ;
- (2) The density  $\rho$  is constant with respect to the trajectory:  $D\rho/Dt = 0$ ;
- (3) The flow conserves volume: the Jacobian  $\det \nabla \Phi^t = 1$ .

The continuity equation can be seen as an extension of incompressible condition, taking compression into consideration. In this case, the conservation law boils down to be

$$\rho \frac{D\phi}{Dt} = \gamma. \quad (10)$$

The conservation law of momentum is more subtle then. On Newtonian fluid profile,  $\gamma$  consists of both body forces (e.g. gravity) and surface forces (stress). The equation for stress, gravity and gravity potential are

$$\tau_{ij} = -P\delta_{ij} + \mu \left( \frac{\partial U_i}{\partial x_j} + \frac{\partial U_j}{\partial x_i} \right), \quad (11)$$

$$\mathbf{g} = -\nabla \psi, \quad (12)$$

$$\psi = gz \quad (13)$$

respectively, where  $\mu$  is the coefficient of viscosity and  $P$  is the pressure. Therefore, using

Einstein notation, if we take gravity into consideration, we have

$$\rho \frac{dU_j}{dt} = -\frac{\partial P}{\partial x_j} - \rho \frac{\partial \psi}{\partial x_j} + \mu \frac{\partial^2 U_j}{\partial x_i \partial x_i}. \quad (14)$$

By defining the *modified pressure*  $p = P - \rho\psi$  and *kinematic viscosity*,

$$\frac{D\mathbf{U}}{Dt} = -\frac{1}{\rho} \nabla p + \nu \nabla^2 \mathbf{U}, \quad (15)$$

which means the gravity term does not matter much.

In all, computational methods for incompressible Newtonian fluids aim to solve

$$\begin{aligned} \frac{D\mathbf{U}}{Dt} &= -\frac{1}{\rho} \nabla p + \nu \nabla^2 \mathbf{U}, \\ \nabla \cdot \mathbf{U} &= 0. \end{aligned} \quad (16)$$

This is the *incompressible Naiver–Stokes equations*.

Additionally, we introduce the notation of *vorticity*, which is defined as

$$\boldsymbol{\omega} = \nabla \times \mathbf{U}. \quad (17)$$

It is clear from definition that vorticity characterized the rate of rotation of the fluid. Conservation law can also be derived for vorticity as

$$\frac{D\boldsymbol{\omega}}{Dt} = \nu \nabla^2 \boldsymbol{\omega} + \boldsymbol{\omega} \cdot \nabla \mathbf{U}, \quad (18)$$

which is also a corollary of incompressible Naiver–Stokes equations. In turbulent flows, a great part of energy is stored in vorticity, and therefore observing distribution of vorticity is of high importance for computational turbulent flows.

## 2.2 Nondimensionalization and Reynolds number

It is clear that the equation (16) owns a great variety of invariance, including time and space invariance, orthogonality invariance and affinity invariance. However, it is not obvious that some similarity invariance is held intrinsically in the incompressible Naiver–Stokes equations.

We perform nondimensionalization first, by selecting characteristic length scale  $\mathcal{L}$  and velocity length scale  $\mathcal{U}$ . By setting  $\hat{\mathbf{x}} = \mathbf{x}/\mathcal{L}$ ,  $\hat{t} = t\mathcal{U}/\mathcal{L}$ , we may define

$$\hat{\mathbf{U}}(\hat{\mathbf{x}}, \hat{t}) = \mathbf{U}(\mathbf{x}, t)/\mathcal{U}, \quad (19)$$

$$\hat{p}(\hat{\mathbf{x}}, \hat{t}) = p(\mathbf{x}, t)/(\rho \mathcal{U}^2). \quad (20)$$

By this mean, (16) can be changed into

$$\begin{aligned}\frac{D\widehat{\mathbf{U}}}{Dt} &= -\frac{1}{Re} \nabla p = \nabla^2 \widehat{\mathbf{U}}, \\ \nabla \cdot \widehat{\mathbf{U}} &= 0.\end{aligned}\tag{21}$$

with the Reynolds number

$$Re = \frac{UL}{v} = \frac{\rho UL}{\mu}.\tag{22}$$

Note that the only constant here is the Reynolds number, and therefore it is the only dependent factor of fluid dynamics. This indicates a Reynolds number similarity can be established also.

As an result, Reynolds number plays a dominant role in turbulent flows according to experiments. It is been verified that Reynolds number greater than 4000 leads to turbulent flows in some cases, while low reynolds number means laminar flows [3]. In engineering, Reynolds number greater than about  $10^4$  is of interest, and therefore turbulent flow problems must be considered.

We will omit the hat on the nondimensionalized quantities for briefness in the following sections.

### 3 Models of direct numerical simulation

#### 3.1 Motivation

The direct numerical simulation (DNS) method is one of the most simplest methods in simulating turbulent flows. To simulate what happens in turbulent flows, we solve the incompressible Naiver–Stokes equations directly (16) (21). This method is the first method developed to simulate turbulent flows, and is also the most accurate method among all the methods. However, since directly solving the incompressible Naiver–Stokes equation costs too much time, this method is rarely used in practice.

#### 3.2 Descretization

There are mainly three descretization techniques toward partial differential equations, say the finite difference method (FD, FDM), the finite volume method (FVM) and the finite element method (FEM).

To apply finite difference method, what we need do first is to discretize the geometric domain into numerical grids. Simple grid parallel to coordinate axes usually applies, but curved grids may also be used for complex geometries. After discretizing the geometric domain, we can utilize difference on the grid to represent the derivatives. An example on the real line is

$$\left. \frac{\partial u}{\partial x} \right|_{x_i} = \frac{u(x_{i+1}) - u(x_i)}{x_{i+1} - x_i} + O((x_{i+1} - x_i)^2),\tag{23}$$

where  $x_{i+1}$  and  $x_i$  are two grid points, and  $u$  is the unknown to be solved. In this way, we can transform the PDE into a difference equation, and then approximate the solution to the PDE by solving the difference equation. Since the finite difference functions space on a bounded set is often of finite dimension, the finite difference equation can be solved by solve an equation of finite variables. This is the finite difference method.

Finite volume method is another category of numerical methods to solve partial differential equations. Similar to the finite difference method, in the finite volume method, the domain is firstly been divided into several control volumes, and what we are going to define is the function value on the boundary or the center of each control volumes.

With integral conservation laws, we can find the integral equations for each control volumes. If we sum up the integral equations respect to all the control volumes, we can obtain a global conservation. Therefore, the main problem in the finite volume method, is to approximate surface integrals and volume integrals of each control volumes. Numerical quadratures and approximations are used here, such as the Simpson formula.

Finite element method is a little bit different to the previous two methods. The main idea of the finite element method is the Galerkin method. That is, instead of solving the PDE directly, we write its variational form, and then try to find its weak solution. The domain is also divided into some regions, and the discretized object function space  $U_h$  and test function space  $V_h$  are piece-wise linear functions. Then what we need to do is to find a approximation solution  $u_h$  in  $U_h$  satisfies

$$\mathcal{L}(u_h, v_h) = 0 \quad (24)$$

for all  $v_h \in V_h$ , which is the discretized variational problem. Noticing that this problem is equations of finite variables, we can solve it by solving equations.

Every time we discretize quantities, errors get involved. Hence, to choose a scheme which owns high-order accuracy and can be solved efficiently is our goal.

### 3.3 Schemes

Schemes needs to carefully designed to numerically solve incompressible Naiver–Stokes equations. One scheme of high popularity is

$$\begin{aligned} \frac{\mathbf{U}^{n+1} - \mathbf{U}^n}{\Delta t} + (\mathbf{U}^n \cdot \nabla) \mathbf{U}^n &= -\frac{1}{\rho} \nabla p^{n+1} + \nu \nabla^2 \mathbf{U}^{n+1}, \\ \nabla \cdot \mathbf{U}^{n+1} &= 0. \end{aligned} \quad (25)$$

This scheme can be considered as backward Euler scheme regardless of the convection term. In this scheme, as for space discretization, we can just choose central space schemes.

This Crank-Nicholson scheme is a more accurate scheme than the previous scheme. The

whole scheme can be described as follows:

$$\frac{\mathbf{U}^{n+1} - \mathbf{U}^n}{\Delta t} + (\mathbf{U}^{n+1/2} \cdot \nabla) \mathbf{U}^{n+1/2} = -\frac{1}{\rho} \nabla p^{n+1} + \frac{\gamma}{2} \nabla^2 (\mathbf{U}^{n+1} + \mathbf{U}^n), \quad (26)$$

$$\nabla \cdot \mathbf{U}^{n+1} = 0.$$

Note that viscosity term is modified. Comparing to the previous scheme, the Crank-Nicholson scheme is half-explicit-half-implicit. This can increase the discretization order in time dimension. Besides, we use a different way to tackle the non-linear term here. The  $n + 1/2$  step in the non-linear term corresponds to

$$(\mathbf{U}^{n+1/2} \cdot \nabla) \mathbf{U}^{n+1/2} = (\mathbf{U}^{n+1} \cdot \nabla) \mathbf{U}^n + (\mathbf{U}^n \cdot \nabla) \mathbf{U}^{n+1} - (\mathbf{U}^n \cdot \nabla) \mathbf{U}^n, \quad (27)$$

which is typical for such coupled problems.

For the partial differential equations which describe the motion of fluid, there is one main difficulty. That is, the equations we solve involves in non-linear terms, and leads to the non-linearity in discretized equations. Hence the previously described method of solving linear equations cannot be applied directly, and we will need some other method to deal with the non-linearity.

For the non-linearity equation, there are two types of way to solve: solving simultaneously or solving sequentially. The former type of method is too expensive to simulate fluid.

Therefore the sequential solution method is the mainstream method and we will go into some details here. The idea of the latter type is to fix some variable to obtain a system of linear equations which we can solve, then update these variable and start another such iteration. As in the sequential solving process, we always solve these linear equations with iterative methods. Thus the whole process contains two parts:

- (1) Fix all the variables involved in coefficients to get a system of linear equations, and then solve these linear equations. Then update the variable in coefficient. Such iterations are called outer iterations.
- (2) Solve the obtained linear equations with iterative methods. And such iterations are called inner iterations.

In order to keep the stability of the outer iteration, we sometimes use under-relaxation trick here.

Newton method is a direct way to solve non-linear equation. The core idea of this method is to use the tangent of  $x_k$  to represent the curve. However, although Newton method enjoys quadratic convergence, it is somehow unstable: the initial guess should always be placed near the real solution. In some extreme cases, convexity also makes a difference. In practice, this method is often combined with other method, to compensate the weakness of it.

### 3.4 Linear system solvers

No matter what method we use to discretize out differential equations, we have to solve the linear equations finally. The following are the most commonly used method in solving linear equations:

- (1) LU decomposition or Gaussian elimination;
- (2) Jacobian iterations;
- (3) Gauss–Seidel iterations;
- (4) Successive over-relaxation (SOR);
- (5) Conjugate gradient (CG) method;
- (6) Incomplete LU decomposition and preconditioned conjugate gradient method (ILUPCG, Stone method);
- (7) Multi-grid method (MGM).

After discretizing the equations, normally we will obtain a system of linear equations, then the previous described methods can be exerted to solve. Some method, such as multi-grid method, enjoys a linear time complexity to the scale of the problem.

## 4 Models of large eddy simulation

### 4.1 Motivation

Even though direct numerical simulation is of great accuracy, the time cost in simulating with that method is extremely high. Engaged with the idea that small motions of the fluid make small contributions in the entire simulations, the large eddy simulation method, which only considers the large scale motions, has been proposed.

### 4.2 Basic model

In order to simply consider the large scale motion, this method first erases all the details of the fluid. That is, any quantity  $\phi$  can be convoluted with a filter kernel  $K(x, x')$  like

$$\bar{\phi}(\mathbf{x}) = \int K(\mathbf{x}, \mathbf{x}') \phi(\mathbf{x}') d\mathbf{x}'. \quad (28)$$

Here the kernel  $G$  should have polishing localized function. Consequently, a local average filter, a band-width filter or a Gaussian kernel may apply. In this equation, there is also a parameter  $\Delta$  which matters. This parameter describes the scale of the filter, which means that the eddy larger whose size is larger than  $\Delta$  will be considered and the one whose size is smaller than  $\Delta$  will be ignored in this method. Obviously  $\Delta$  should be larger than the grid size, but usually no other restriction is forced.

Equipped with this, we convolve the incompressible Naiver–Stokes equations with the filter

kernel to obtain

$$\frac{\partial(\bar{U}_i)}{\partial t} + \frac{\partial(\bar{U}_i \bar{U}_j)}{\partial x_j} = -\frac{1}{\rho} \frac{\partial \bar{p}}{\partial x_i} + \nu \frac{\partial}{\partial x_j} \left[ \left( \frac{\partial \bar{U}_i}{\partial x_j} + \frac{\partial \bar{U}_j}{\partial x_i} \right) \right]. \quad (29)$$

According to the linearity of the continuity equation and incompressibility, we also have

$$\frac{\partial(\bar{U}_i)}{\partial x_i} = 0. \quad (30)$$

Since the second term in the left of (29) is hard to computed, we introduced the *subgrid-scale Reynolds stress* (SGS Reynolds stress) in (31) to handle this. The subgrid-scale Reynolds stress is defined as

$$\tau_{ij}^s = -(\bar{U}_i \bar{U}_j - \bar{U}_i \bar{U}_j). \quad (31)$$

As soon as we determine the value of  $\tau_{ij}^s$ , we can solve (29) numerically, and this gives solutions of speed field after convolution. Among these solutions, the motions of large eddies will be considered and the motion of small eddies will be ignored.

However, there is no direct solution to the filtered equations, because the equations are not closed, meaning that the number of variables is more than the number of equations. To be exact, the variables include  $\bar{U}_i$ ,  $\bar{p}$  and  $\bar{U}_i \bar{U}_j$ , the number of which is greater than 4, the number of equations. Therefore, we need to add some restrictions on the sub-grid scale Reynolds stress, and this leads to several different models which will be introduced later. Major models include the Smagorinsky model, the dynamic model and the deconvolution model. Before we introduce the Smagorinsky model, the filtered rate of strain will be defined first.

For the filtered velocity field  $\bar{\mathbf{U}}$ , we can define the tensor of filter rate of strain as follows:

$$\bar{S}_{ij} = \frac{1}{2} \left( \frac{\partial \bar{U}_i}{\partial x_j} + \frac{\partial \bar{U}_j}{\partial x_i} \right). \quad (32)$$

Additionally, the filter rate of strain  $\bar{S}$  is defined by

$$\bar{S} = \sqrt{2 \bar{S}_{ij} \bar{S}_{ij}}, \quad (33)$$

using Einstein notation. This value is correlated to the energy function.

### 4.3 Smagorinsky model

Based on eddy viscosity, Smagorinsky proposed a model in 1963. The core idea of this model is that we restrain our sub-grid scale Reynolds stress in accordance to (34)

$$\tau_{ij}^s - \frac{1}{3}\tau_{kk}^s\delta_{ij} = \nu_t \left( \frac{\partial \bar{U}_i}{\partial x_j} + \frac{\partial \bar{U}_j}{\partial x_i} \right) = 2\nu_t \bar{S}_{ij} \quad (34)$$

This equation can be derived from equation production and dissipation of kinetic energy, which needs further statistical hypothesis. Here  $\nu_t$  represents the eddy viscosity, and should be chosen as

$$\nu_t = C_s^2 \rho \Delta^2 \bar{S}, \quad (35)$$

where  $C_s$  is the model parameter, and  $\Delta$  is the size of the filter. The parameter  $C_s$  is not constant. Instead, it is selected based on the Reynolds number, and it may be different in different types of fluid. In the Smagorinsky model, the value of  $C_s$  varies from 0.2 to 0.065. The smaller it is, the less eddy viscosity the simulated profile has.

### 4.4 Dynamic model

The Smagorinsky model has one crucial problems, that is, the proper value of  $C_s$  varies among different type of fluid. To be exact,  $C_s$  should be zero in laminar flow, and should be small near the wall and should be large at where Reynolds number is large. This parameter is hard to determine, and the dynamic models proposed a convenient and efficient way to model.

Except for the original filter  $K$ , this model introduces another filter  $\tilde{K}$ , whose size  $\tilde{\Delta}$  is larger than the original size  $\Delta$ . This means the filter  $\tilde{K}$  is coarser than the original filter, and we are going to adopt the information we obtained after we exert this coarse filter to determine the Smagorinsky coefficient  $C_s$ .

According to the previous notations, the original velocity is  $\mathbf{U}$  and the velocity after convolution with the filter  $K$  is  $\bar{\mathbf{U}}$ . Here we use  $\widetilde{\mathbf{U}}$  to denote the velocity field obtained by exerting convolution with  $\tilde{K}$  on  $\bar{\mathbf{U}}$ . In this way, we define

$$T_{ij} = - \left( \widetilde{\bar{U}_i \bar{U}_j} - \widetilde{\bar{U}_i} \widetilde{\bar{U}_j} \right), \quad (36)$$

$$L_{ij} = T_{ij} - \widetilde{\tau_{ij}} = - \left( \widetilde{\bar{U}_i \bar{U}_j} - \widetilde{\bar{U}_i} \widetilde{\bar{U}_j} \right). \quad (37)$$

Here the value  $L_{ij}$  is called *resolved stress* and can be calculated only in terms of  $\bar{U}_i$ . According

to (34) and (35), we have

$$\tau'_{ij} = \tau_{ij} - \frac{1}{3}\tau_{kk}\delta_{ij} = 2C_s\Delta^2 \bar{S}\bar{S}_{ij}, \quad (38)$$

$$T'_{ij} = T_{ij} - \frac{1}{3}T_{kk}\delta_{ij} = 2C_s\tilde{\Delta}^2 \tilde{\bar{S}}\tilde{\bar{S}}_{ij}. \quad (39)$$

Based on the approximation

$$L_{ij} - \frac{1}{3}L_{kk}\delta_{ij} \approx T'_{ij} - \widetilde{\tau'_{ij}}, \quad (40)$$

if we define

$$M_{ij} = 2\Delta^2 \widetilde{\bar{S}}\widetilde{\bar{S}}_{ij} - 2\tilde{\Delta}^2 \tilde{\bar{S}}\tilde{\bar{S}}_{ij} \quad (41)$$

then we obtain

$$L_{ij} - \frac{1}{3}L_{kk}\delta_{ij} \approx C_s M_{ij}. \quad (42)$$

Therefore, we can determine the value of  $C_s$  by

$$C_s = \frac{M_{ij}L_{ij}}{M_{kl}M_{kl}}. \quad (43)$$

To remove the fluctuation in calculating  $C_s$  based on the formula (43), we can calculate the average value in the numerator and denominator in (43). This method has been proved to lead to good calculations.

Though this model presents an tractable way to simulate turbulent flows approximately, there are still many weaknesses and difficulties in it, such as inaccuracy.

## 4.5 Deconvolution Models

This model is different to the previous two models. The core idea is to calculate the unfiltered velocity field according to the filtered velocity field. If we have the unfiltered velocity, then we can compute the sub-grid scale Reynolds stress directly. In this way, the problem is how can we estimate the unfiltered velocity.

We first expand (28) in a Taylor series at a point  $\mathbf{x}$  and only keep the first order term and the second order term. This will provide us a differential equation for the unfiltered velocity. Suppose the filter kernel is symmetric for  $\mathbf{x}$ , then the differential equation can be write as:

$$\bar{u}_i = u_i + \frac{\Delta^2}{24} \nabla^2 u_i. \quad (44)$$

To solve this equation, finding the approximate inversion is an appropriate idea. Katapodes' method

$$u_i \approx \bar{u}_i - \frac{\Delta^2}{24} \nabla^2 \bar{u}_i \quad (45)$$

applies here.

## 5 Models of Reynolds-averaged simulation

### 5.1 Motivation

The advantages of the previously described methods, the direct numerical simulation method or the large eddy simulation method, is that they contain many information of fluid and are much accurate to real situation. However, people usually focus on the average forces exerted on the fluid or the degree of mixing two streams of fluid. Thus most of the information they provided is redundant or useless. A century ago, Reynolds proposed the Reynolds-averaged simulation (RAS) model, aiming to simulate the average motion of fluid.

This model does not provide information which is not useful, and because of this, this model requires much less calculations than the previous two models. Therefore, this model is one of the most commonly used model in turbulent simulation.

### 5.2 Basic model

Firstly for every variable, we can write it as the sum of its locally time-averaged value and a residue value as follows:

$$\phi(\mathbf{x}, t) = \langle \phi \rangle(\mathbf{x}) + \phi'(\mathbf{x}, t). \quad (46)$$

Here  $\langle \phi \rangle$  is the average value of  $\phi$ , which is defined as follows:

$$\langle \phi \rangle(\mathbf{x}) = \frac{1}{T} \int_t^{t+T} \phi(\mathbf{x}, s) ds, \quad (47)$$

where  $T$  is an interval shorter than our interest. To find the stable solution, we may consider  $T \rightarrow +\infty$ . One may also consider the effect of chaos into consideration, and in this case  $\langle \phi \rangle$  represents the expectation of  $\phi$  under chaotic effect of initial values. The formula in (46) is called *Reynolds decomposition*.

For the next step, we are going to give the definition of Reynolds stress. Note that

$$\langle U_i \rangle \phi = \langle (\langle U_i \rangle + U'_i)(\langle \phi \rangle + \phi') \rangle = \langle U_i \rangle \langle \phi \rangle + \langle U'_i \phi' \rangle. \quad (48)$$

The last term in (48) is zero if and only if  $\phi'$  and  $U'_i$  are uncorrelated, and this situation rarely happens. Hence the *turbulent scalar flux*  $\rho \langle U'_i \phi' \rangle$  need to be introduced. If we take  $U_j$  in the previous equation, then we obtain the *Reynolds stress*,  $\rho \langle U'_i U'_j \rangle$ . The Reynolds stress plays a similar role to sub-grids scale Reynolds stress in large eddy simulation method, although historically Reynolds stress was introduced earlier. Reynolds stress is the main part to be dealt with.

If we take the Reynolds average of incompressible Naiver–Stokes equation, we can obtain

the Reynolds-averaged Naiver–Stokes equation:

$$\frac{\partial \langle U_i \rangle}{\partial x_i} = 0, \quad (49)$$

$$\frac{\partial \langle U_i \rangle}{\partial t} + \frac{\partial}{\partial x_j} \left( \langle U_i \rangle \langle U_j \rangle + \langle U'_i U'_j \rangle \right) = -\frac{1}{\rho} \frac{\partial \langle p \rangle}{\partial x_i} + \frac{\partial \langle \tau_{ij} \rangle}{\partial x_j}, \quad (50)$$

where  $\langle \tau_{ij} \rangle$  are the mean viscous tensor elements as

$$\langle \tau_{ij} \rangle = \nu \left( \frac{\partial \langle U_i \rangle}{\partial x_j} + \frac{\partial \langle U_j \rangle}{\partial x_i} \right). \quad (51)$$

Similar to LES model, the existence of Reynolds stress and turbulent scalar flux also means that the equations are not closed and hence impossible to solve directly. Therefore, we need some restrictions and correlations on them. And this give rise to the following two models: the  $k-\epsilon$  model and the v2f model.

### 5.3 $k-\epsilon$ model

Since the energy dissipation and the transportation of mass link to the viscosity, we can simply assume that the effect of turbulent flows is represented by an increased viscosity. This leads to the turbulent viscosity model

$$\langle U'_i U'_j \rangle = \nu_t \left( \frac{\partial \langle U_i \rangle}{\partial x_j} + \frac{\partial \langle U_j \rangle}{\partial x_i} \right) - \frac{2}{3} \delta_{ij} k, \quad (52)$$

where  $\nu_t$  is the turbulent viscosity, and  $k$  is the turbulent kinetic energy:

$$k = \frac{1}{2} (\langle U'_x U'_x \rangle + \langle U'_y U'_y \rangle + \langle U'_z U'_z \rangle). \quad (53)$$

According to the turbulent viscosity model, we can obtain the effective viscosity as

$$\nu_{\text{eff}} = \nu + \nu_t. \quad (54)$$

Notice that if we specify  $\mu_t$  and  $\Gamma_t$ , then we can find the solution to  $\langle \mathbf{U} \rangle$  according to the averaged incompressible Navier-Stokes equations, with  $\nu_{\text{eff}}$  replacing  $\nu$  and  $\langle p \rangle + \frac{2}{3} \rho k$  replacing  $p$ . The transformed equations have identical structure to incompressible Navier-Stokes equations, and similar solving techniques can be adopted.

Next we will talk about how to determine the value of  $\mu_t$ . In the simplest model, we can just do the dimensional analysis and try to determine these parameters. In this way,  $\mu_t$  can be characterized by

$$\mu_t = C_\nu \rho q L, \quad (55)$$

where  $C_v$  is a dimensionless constant,  $L$  is the length scale of the turbulent flows and  $q$  here is a velocity with  $q = \sqrt{2k}$ . In order to determine  $L$ , the most popular model involves the dissipation term  $\epsilon$ . This model constrains the  $L$  as

$$\epsilon = \frac{k^{3/2}}{L}. \quad (56)$$

Therefore, the turbulent viscosity is

$$\nu_t = \rho C_v \frac{k^2}{\epsilon}. \quad (57)$$

Commonly the value  $C_v$  is chosen as  $C_v = 0.09$ . Equipped with this, we can finish the calculation. This model is called  $k-\epsilon$  model.

## 5.4 v2f Model

There is a problem with the above model, which is that the proper condition near the wall is not known. And the changes of the kinetic quantities and the dissipation are very fast so that we cannot find a appropriate model to characterize them clearly. And the main difficulty in the region near a wall is that some quantity will be too near to zero. Such quantity is the normal velocity  $\mathbf{V}$  and the fluctuation normal velocity  $V'^2$ . And this model aims to deal with this, and can perform better while the cost is nearly the same with  $k-\epsilon$  model.

# 6 Comparison between models

## 6.1 Analysis

In this section, we will compare the previously described three models, and analyze the advantages and disadvantages of them.

For the direct numerical simulation method, it is the most easy one to implement, since the idea of DNS method is to simulate the fluid directly. Hence this method is not only adaptive to turbulent simulation, but also to all types of fluid. Besides, since we do not make any approximation to the model, this model is the most accurate model in simulating turbulent flows. However, this model has some vital weakness, that is, the calculation of numerical simulation is so time costly that this model cannot been used in practice.

Some qualitative calculation can also be carried out. According to the theory of Kolmogorov, the grid size  $\Delta$  must be smaller than the scale of dissipation, and the region size  $L$  must be greater than the scale of energy. This means that the density of grids on one axis

$$N = L/\delta > O(\text{Re}^{3/4}), \quad (58)$$

where the power  $3/4$  results in the ratio of scales in energy cascade models [6]. This means the number of cube grids is at least  $N^3 > O(\text{Re}^{9/4})$ . According to CFL condition, the Courant

number should be controlled below 1, and therefore near linear correlation between time step and space step is required. This further implies that the complexity is at least

$$N^4 > O(\text{Re}^3). \quad (59)$$

As mentioned before, in real world engineering,  $\text{Re}$  is usually no less than  $10^4$ , and this is nearly impossible in a short period even with clusters. It should be emphasized that grids contradicting above constraint cannot capture turbulent flows appropriately, and therefore coarse grids do not make sense here.

The large eddy simulation method is an approximation model. With the idea that the small turbulent flows are insignificant to energy transportation and material exchanges, this model points out a way to eliminate the effect of small turbulent flows. Thus only large turbulent flows need to be calculated in this model, and small turbulent flows are directly modeled. This simple movement give rise to much reduction in time complexity. However, since some approximation have been added on this model, the accuracy of the solution must have been deteriorated. However, the result of the fluid does not changed a lot, for only the non-essential details have been lost. Besides, though this model save much time from the DNS model, it is still so time costly that only simulation and examination, or some small scale simulation problems can be done with this method. Directly solving the turbulent simulation for large scale fluid still seems not possible.

Reynolds-averaged simulation is the most well-used method in turbulent simulation. Equipped with the idea that people usually only care about the movement of fluid in long time average, this method divided the motion of fluid into the average motion and the fluctuation. What this method focuses on is to find a solvable PDE for the average motion. This idea brings to the definition and analysis of Reynolds stress. In general, the Reynolds-averaged simulation method does not take much time, but from the solving process we know that the details among the time step will be lost. Thus this method is far away from the accurate methods, but it points out an available way to describe the movement of fluid in acceptable time. Therefore in the real time, only the time cost of Reynolds-averaged simulation permits us to find solution for turbulent simulation. In addition, Reynolds-averaged simulation method can handle “near steady” cases, in which the flow is not steady at all but statistical stability may be utilized.

In real world engineering, it is important to find a trade off between accuracy and efficiency. Therefore, Reynolds-averaged simulation enjoys high popularity. However, as the computational capability of computer increases, large eddy simulation methods attract more and more attention. Although direct numerical simulation is usually intractable, it is the golden standard for verification. [11]. Due to the defects of these models, it is still a problem to increase either accuracy or efficiency and attain a better trade off nowadays.

Comparison between these models, and algorithms are summarized in Table 1.

Table 1 Comparison between models and algorithms

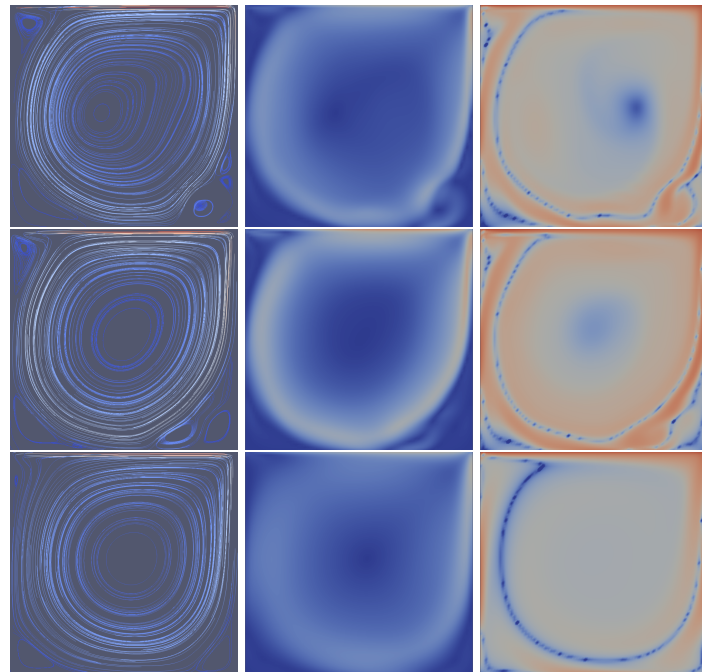
	DNS	LES	RAS
Accuracy	High, standard	Medium	Low, acceptable
Efficiency	Low, unacceptable	Medium	High
Grid size	Dense	Relatively coarse	Relatively coarse
Time step	Small	Relatively large	Relatively large
Feature	High accuracy	Multi-scale capability	Handle statistical steadiness

## 6.2 Experiments

We will examine two well acknowledged profile here. The experiments are carried out originally.

The first numerical experiment is about the lid-driven cavity problem [1]. In this problem, a 2-dimensional square box having three fixed walls and a moving wall is filled with fluids. The size of the box is 0.1 m, and the velocity of moving wall is set to be  $1 \text{ m s}^{-1}$ . The kinetic viscosity  $\nu$  is chosen to be  $10^{-5} \text{ m}^2 \text{ s}^{-1}$  to achieve the Reynolds number  $\text{Re} = 10^4$  here.

The results at 5 s of  $80 \times 80$  grid is shown in Figure 1. For large eddy simulation, the basic Smagorinsky model is used. For Reynolds-averaged simulation,  $k-\epsilon$  model is used.

Figure 1 Simulation results at 5 s for  $80 \times 80$  grid

First row: DNS, second row: LES, last row: RAS. First column: flow stream lines; second column: magnitude of flow velocity  $\mathbf{U}$ ; third column: logarithm of magnitude of vorticity  $\omega$ . Blue means smaller quantities and red means larger. Best viewed in color and on digital display. (Digital version of this report can be found in <https://github.com/pppppass/TurbulentFlow/Report/Report.pdf>)

From this figure, it can be easily verified that direct numerical simulation owns the highest

accuracy: small structures of vortexes are kept. Large eddy simulation removes some small structure, while Reynolds-averaged simulation erased patterns of small scale almost completely.

However, to study the difference of efficiency, we have to study the dynamics of these models and algorithms. The dynamic from 1 s to 5 s is shown in Figure 2.

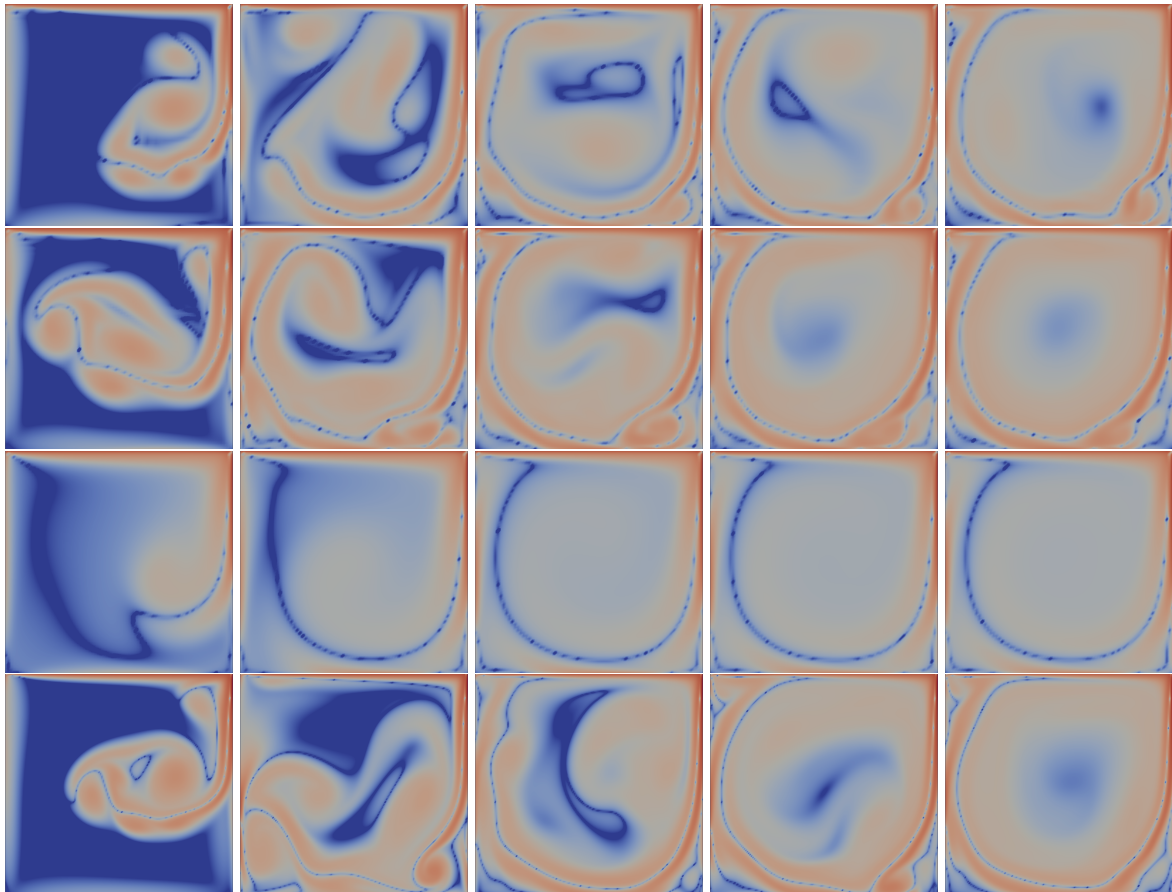


Figure 2 Simulation dynamics from 1 s to 5 s

This is figures of logarithm of magnitude of vorticity  $\omega$ . First row: DNS for  $80 \times 80$  grid; second row: LES for  $80 \times 80$  grid; third row: RAS for  $80 \times 80$  grid; fourth row: DNS for  $160 \times 160$  grid. Columns from left to right represent 1, 2, 3, 4, 5 s respectively. Blue means smaller quantities and red means larger. Best viewed in color and on digital display.

From this figure, it can be directly observed that the direct numerical simulation on coarse grids does not converge into the stable solution rapidly. On the contrary, the solution of large eddy simulation and Reynolds-averaged simulation converges faster because of the introduction of space or time averaging. It is clear that Reynolds-averaged simulation gets stable in two seconds, and this proves that this simulation method can capture statistical steadiness. Another important comparison is between the first, second and fourth row: the result of direct numerical simulation on the fine grid is more similar to the result large eddy simulation on the coarse grid, especially at 1 s and 5 s. This tells the success of multi-scale modeling of large eddy simulation: the structures of small scales are directly modeled rather than computed, and

therefore it is possible to simulation on a coarse grid using large eddy simulation as if direct numerical simulation is performed on a fine grid. This highly increases efficiency and cuts down computations.

We summarize the running time for different simulation methods and grid sizes. This is shown in Table 2.

Table 2 Comparison on running time (s)

Grid size	DNS	LES	RAS
$20 \times 20$	4.62	5.19	6.16
$40 \times 40$	21.84	25.56	28.20
$80 \times 80$	161.82	174.46	198.67
$160 \times 160$	1380.04	1564.41	1890.42

Because the number of equation gets larger for large eddy simulation and Reynolds-averaged simulation, the running time also becomes longer. However, one should not forget about the grid size: from previous argument, large eddy simulation behaves well on coarse grid, and significantly cuts down the running time. For Reynolds-averaged simulation, the system gets stable in a fast sense, and the simulated time can also be noticeably decreased.

We examine the example of flow over a cylinder. The cylinder of fluids 0.5 m is placed into a 2-dimensional rectangular flow pipe of width 2 m. The center of cylinder section is 2 m to the inlet and 18 m to the outlet. The inlet provides flow of velocity  $U_0 = 1 \text{ m s}^{-1}$ . To break the symmetry, we add  $U'_0 = 0.1 \text{ m s}^{-1}$  vertically. The kinetic viscosity is  $5 \times 10^{-4} \text{ m s}^{-1}$ . As a result, the Reynolds number is about 3000 (considering the half upper region and ignore  $U'_0$ ).

The simulation result is shown in Figure 3. Kármán vortex street can be observed.

In this figure, the distinction between these three models are again magnified. The comparison the first two rows shows that the vortex street of large eddy simulation is more regular and continuous, while that of direct numerical simulation introduces some artifacts here. To be exact, the vortex street in direct numerical simulation gets broken up and the size of vortexes varies a lot. This is because the size of grids does not reach the Reynolds number, as mentioned before, and therefore direct numerical simulation cannot capture such details. For large eddy simulation, part of the vortexes are modeled and therefore accuracy and regularity can be preserved. Note that Reynolds-averaged simulation fails here, because the profile itself does not own statistical steadiness: it has periodical movement after all.

These results are carried out on a computer with Intel Core i7-6500U (4 threads) and 7886 MiB RAM. The operating system is Arch Linux 4.16.13 64-bit. We deploy OpenFOAM [9] for numerical simulation. Detailed settings include initial values, boundary conditions and numerical schemes are provided in <https://github.com/pppppass/TurbulentFlow/Experiments>.

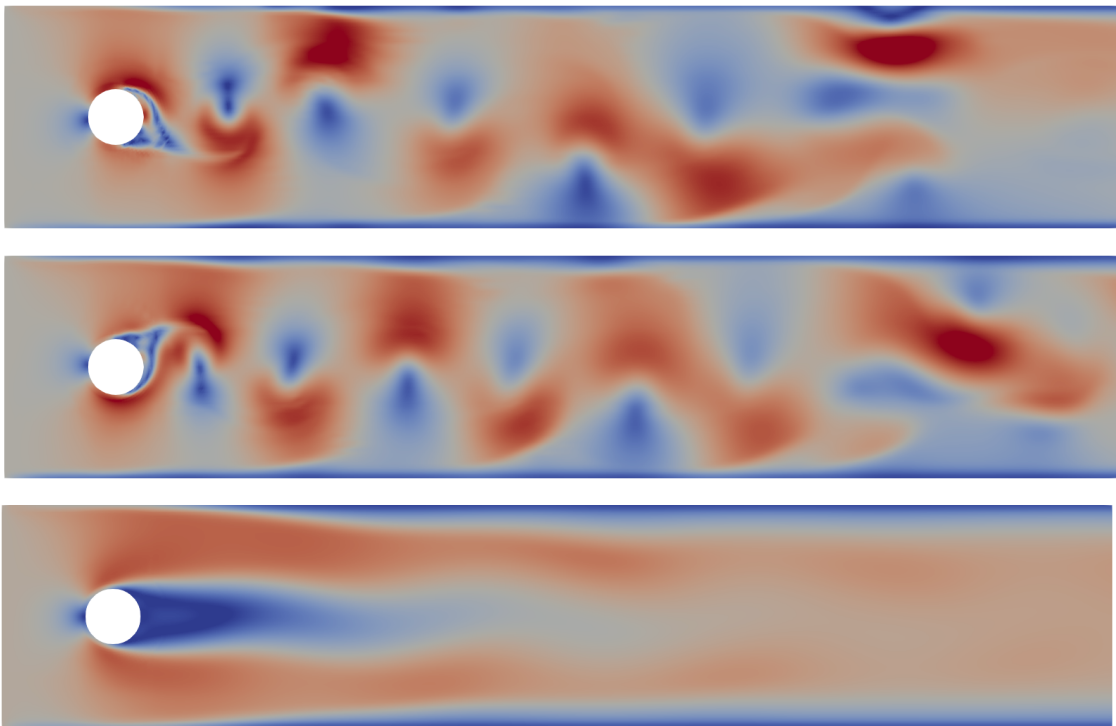


Figure 3 Simulations result of flows over a cylinder at 20 s

This is figures of magnitude of flow velocity  $\mathbf{U}$ . First row: DNS; second row: LES; last row: RAS. Blue means smaller quantities and red means larger. Best viewed in color and on digital display.

## 7 Conclusion

This report presents an introduction to turbulent simulation, including the mathematical formulation and three different models: direct numerical simulation, large eddy simulation and Reynolds-averaged simulation. Comparison among these three models are also showed in this report. We also present detailed analysis and numerical experiments on various cases with these three models, and show the distinctions among these models.

Turbulent flows are of high importance in computational mathematics and engineering. It is also an interesting question whether it is possible to combine classical models with recent popular learning-based algorithms. One of the key challenge for learning-based algorithms is to “learn” the model directly. After all, in some sense, the problem of turbulent flows is main a problem of models.

## 8 Acknowledgement

Ten days ago, we had no acquaintance with anything in the field of computational fluid dynamics and turbulent flows simulation at all. Although we finished the literature survey and comparative analysis and experiments on our own, we express our thanks to Zexing Li, whose talk initiated us to begin such an adventure.

## 9 Reference

### References

- [1] Charles-Henri Bruneau and Mazen Saad. “The 2D lid-driven cavity problem revisited”. In: *Computers & Fluids* 35.3 (Mar. 1, 2006), pp. 326–348. ISSN: 0045-7930. doi: [10.1016/j.compfluid.2004.12.004](https://doi.org/10.1016/j.compfluid.2004.12.004).
- [2] Joel H. Ferziger and M. Peri. *Computational methods for fluid dynamics*. 3rd, rev. ed. Berlin ; New York: Springer, 2002. 423 pp. ISBN: 978-3-540-42074-3.
- [3] J. P. Holman. “Heat transfer, 1986”. In: *Mc GranHill Book Company, Sothern Methodist University* (1986).
- [4] Andrej Nikolaevich Kolmogorov. “Equations of turbulent motion in an incompressible fluid”. In: *Dokl. Akad. Nauk SSSR*. Vol. 30. 1941, pp. 299–303.
- [5] L. D. Landau and E. M. Lifshitz. *Fluid Mechanics, Second Edition: Volume 6*. 2 edition. Amsterdam u.a: Butterworth-Heinemann, Jan. 15, 1987. 552 pp. ISBN: 978-0-7506-2767-2.
- [6] Stephen B. Pope. *Turbulent flows*. IOP Publishing, 2001.
- [7] Katepalli R. Sreenivasan. “On the universality of the Kolmogorov constant”. In: *Physics of Fluids* 7.11 (Nov. 1, 1995), pp. 2778–2784. ISSN: 1070-6631. doi: [10.1063/1.868656](https://doi.org/10.1063/1.868656).
- [8] G. I. Taylor. “Diffusion by Continuous Movements”. In: *Proceedings of the London Mathematical Society* s2-20.1 (), pp. 196–212. ISSN: 1460-244X. doi: [10.1112/plms/s2-20.1.196](https://doi.org/10.1112/plms/s2-20.1.196).
- [9] H. G. Weller et al. “A tensorial approach to computational continuum mechanics using object-oriented techniques”. In: *Computers in Physics* 12.6 (Nov. 1, 1998), pp. 620–631. ISSN: 0894-1866. doi: [10.1063/1.168744](https://doi.org/10.1063/1.168744).
- [10] Frank M. White. *Fluid Mechanics Fourth Edition*. McGraw-hill, 2017.
- [11] Zhaoshun Zhang, Guixiang Cui, and Chunxiao Xu. *Theory and Modeling of Turbulence*. Tsinghua University Press, 2005.